sustainability

MDPI

Article

Modeling and Analysis of Electric Vehicle-Power Grid-Manufacturing Facility (EPM) Energy Sharing System under Time-of-Use Electricity Tariff

Xiaolin Chu [1], Yuntian Ge [2], Xue Zhou [2], Lin Li [2,*] and Dong Yang [3]

[1] School of Financial Technology, Shanghai Lixin University of Accounting and Finance, Shanghai 201209, China; cxlin2016@126.com
[2] Department of Mechanical and Industrial Engineering, University of Illinois at Chicago, Chicago, IL 60607, USA; yge20@uic.edu (Y.G.); zhouxue@uic.edu (X.Z.)
[3] Glorious Sun School of Business and Management, Donghua University, Shanghai 200051, China; yangdong@dhu.edu.cn
* Correspondence: linli@uic.edu; Tel.: +1-312-9963405

Received: 17 May 2020; Accepted: 11 June 2020; Published: 13 June 2020

Abstract: Electric vehicles (EVs) have obtained increasing public interest due to the associated economic and environmental benefits. Recently, studies regarding the economic advantages of adopting EVs as energy storages for commercial/residential buildings are emerging. In fact, according to the U.S. Energy Information Administration, the industrial sector consumes more energy than all of the other sectors combined, which is about 54% of the world's total delivered energy. The energy consumption pattern in manufacturing facilities is based on production schedules and the heat transfer between machines and the ambient surroundings, thus, differs greatly from commercial/residential buildings. However, little research attention has been given to analyse the synergies of integrating EVs and manufacturing facilities to improve energy efficiency. To fill this research gap, in this study, a comprehensive model is established to evaluate the economic and environmental performance of an energy sharing system that consists of the EVs, power grid, and manufacturing facilities (EPM) under Time-of-Use (TOU) electricity tariff. The model is formulated as a mixed integer nonlinear programming format by considering practical production schedules, heat exchange between machines and ambient surroundings, as well as the heating, ventilation, and air conditioning (HVAC) system. The case study results indicate that the presented EPM energy sharing system has great potential to reduce energy cost and CO_2 emissions. In addition, compared to the results from winter scenarios, it is shown that more cost savings can be achieved in summer days.

Keywords: electric vehicles; smart grid; manufacturing facility; time-of-use electricity tariff; cost modelling

1. Introduction

From 1980 to 2018, worldwide greenhouse gas (GHG) emissions increased by 95% [1]. In terms of infrastructures, the industry and transportation sectors are the top two GHG emission contributors, accounting for 21% and 14% of the total GHG emission, respectively [2]. As global warming is becoming a serious concern and a threat to future generations [3], countries around the world have made various efforts since the Paris Agreement to reduce GHG emissions, e.g., promoting sustainable manufacturing [4], improving energy efficiency [5], and using non-fossil energy sources [6]. In particular, the adoption of electric vehicles (EVs) to replace conventional gasoline vehicles is widely considered as an effective method to reduce the GHG emission [7].

Compared to conventional vehicles with combustion engines, the application of EVs can reduce the national dependency on fossil fuels, improve energy efficiency and reduce carbon dioxide (CO_2) emissions [8,9]. As a result, EVs have obtained growing attention worldwide. Subsequently, the global EV market increased by 65% from 2017 to 2018 [10]. Moreover, nearly 2.7 million EVs are anticipated to be on the road in the U.S. by 2020 [11]. However, the large adoption of EVs brings challenges to the power grid stabilization due to the current lack of supporting infrastructures and difficulties in overcoming technological barriers. For example, the electricity consumption rate of EVs is around three times more than the average household electricity consumption rate, which can overload the power grid, especially during peak demand hours [12]. The existing electricity infrastructure might not be capable of providing enough power to satisfy the surge in power demand [13].

To alleviate the excessive load and further enhance the economic and environmental sustainability of power grid, a modern power grid infrastructure used to improve the utilization of real time communications technology has emerged [14]. It is also referred to as the "vehicle-to-grid" (V2G) operation, which is a bi-directional communication and electricity flow between EVs and the power grid [15]. Although the V2G application may increase the number of charge–discharge cycles and reduce the useful life of battery, the EV batteries can be reused in homes or other business applications as an energy storage device to extend the life cycle [16]. In addition, there are substantial benefits to adopting V2G operation. For the power grid, the V2G operation has the potential to enhance operation and control in power systems by providing additional flexibility [17]. On the other hand, for customers, EVs can be considered as dispersed energy storages to achieve monetary savings by shifting power usages from on-peak demand to off-peak demand periods [18]. Extensive research efforts have been devoted to the V2G integration regarding systematic design and optimization [19–21], economic performance improvement [22–25], environmental sustainability evaluation [7,24,26], etc. For example, Iacobucci et al. developed a simulation-based model to examine the potential of V2G integration using shared autonomous EVs and found that demand–response strategies can significantly decrease cost of the system [27]. In addition, Bashash et al. proposed a convex quadratic programming framework for the charging pattern optimization of plug-in hybrid electric vehicles under time-varying electricity price signals and demonstrated that an adequate fuel economy could be achieved via the proposed V2G integration [28]. Furthermore, Sarker et al. established a centralized model to improve the transformer loss-of-life with the benefits for EVs' owners on charging/discharging management [29].

With the increasing adoption of EVs, studies regarding the economic benefit of energy sharing between EVs and other energy end users have been emerging. Vehicle-to-building (V2B) technology is proposed to reduce the energy cost of buildings and EVs [30] and provide multiple power sources, higher electricity quality for buildings, and peak power shaving by demand side management [31], as well as reduce the CO_2 emissions [32]. Most recent studies are focused on promoting the energy communication strategies between EVs and commercial/residential buildings [33–39]. Quddus et al. developed a collaborative decision model to study energy sharing among buildings and charging stations and achieved 14.24% overall energy cost reduction [40]. Moreover, Wang et al. developed a V2B energy sharing scheme to improve the power supply reliability and comfort management for smart buildings [41].

However, in current literature, few research efforts are dedicated to studying the energy sharing and collaboration between EVs and industrial facilities. As the largest energy user and GHG emission contributor, in the industrial sector, manufacturing activities account for 90% of the energy consumption and 84% of the energy-related CO_2 emissions [42]. In fact, there are many differences in energy management methods between manufacturing facilities and commercial/residential buildings. For example, the electricity demand curve is determined by the production schedule in manufacturing systems by applying electricity demand management. The heating and cooling energy demand to manage a facility's indoor temperature can be changed by taking into account the convective and radiant heat transfer from the manufacturing operation [43]. Therefore, existing methods for V2B operation are not completely applicable in the EVs in manufacturing operations. It is important and

necessary to comprehensively consider the energy sharing between EVs, the power grid, and the manufacturing facility (EPM) from a systematic view.

To fill this research gap, in this study, the concept of vehicle-to-manufacturing (V2M) bidirectional communication operation is proposed to reduce energy cost and GHG emissions for industry facilities and EVs. With the application of a smart garage, the EV charging/discharging control system and infrastructure are widely available. Therefore, the V2M model is viable in real life. Based on this V2M model, a comprehensive EPM energy sharing system is established, in which the electric power exchanges between EVs and the manufacturing facility when EVs are parked and connected to the power grid. A collaborative operation decision model is presented for the EPM energy sharing system to quantify the cost saving, carbon dioxide emission (CDE) reduction and primary energy consumption (PEC) decrease.

In this paper, it is assumed that the EVs of the industrial practitioners arrive at the parking area in the morning and leave in the afternoon or evening. In addition, the manufacturing facility is assumed to have a serial production line with multiple machines and buffers, which is the most common structure in manufacturing plants [44]. It is also assumed that the manufacturing facility adopts a Combined Cooling, Heating and Power (CCHP) system as self-sufficient generation system. The objective is to obtain optimized solutions for the EPM energy sharing system under Time-of-Use (TOU) electricity rates by minimizing the total cost under the constraints of production throughput target, EVs battery demand and energy balance. A mixed integer nonlinear programming (MINLP) collaborative decision model is established and solved by a particle swarm optimization (PSO) algorithm. In the case studies, one-shift and two-shift scenarios are investigated to illustrate the applicability and effectiveness of the presented model. Furthermore, the environmental and energy evaluations of the optimal schedule solution are conducted.

The rest of this paper is organized as follows. The problem description is provided in Section 2. In Section 3, a novel collaborative decision model is formulated to depict the energy sharing in the EPM system. The solving procedures to achieve the optimal solution of the model via a PSO algorithm is presented in Section 4. The numerical results from the case studies for the proposed EPM energy sharing system compared to the baseline cases under the TOU tariff are reported in Section 5. Finally, Section 6 gives the conclusions and offers future research directions.

2. Problem Description

In this section, the EPM energy sharing system consisting of the power grid, manufacturing facility, and EV charging stations is proposed to improve the overall energy efficiency. The electricity, heating, and cooling loads of manufacturing facility are supplied from CCHP system, power grid, and/or EVs. The electricity demands of EVs are satisfied by the power grid and manufacturing facility.

The structure of the EPM energy sharing system is presented in Figure 1. The solid lines show the electrical energy flows and the dashed lines signify the heating/cooling energy flows. In relation to manufacturing facility, electricity demand is supplied from power generation unit (PGU) by adopting a gas turbine as a prime mover. The heating demand is fulfilled by the waste heat of the PGU and/or heat from an auxiliary boiler through a heat exchanger. An absorption chiller using a heating source to generate cooling energy is applied as the cooling component in the CCHP system. The absorption chiller takes pure water as the refrigerant and uses lithium bromide (LiBr) solution as the absorbent. In the charging station, EVs can be charged or discharged when connected to the power grid by bidirectional electricity flow. The manufacturing facility can sell its surplus electricity to the power grid and/or sent to EVs, while EVs can share redundant electricity with manufacturing facility or sell back to power grid.

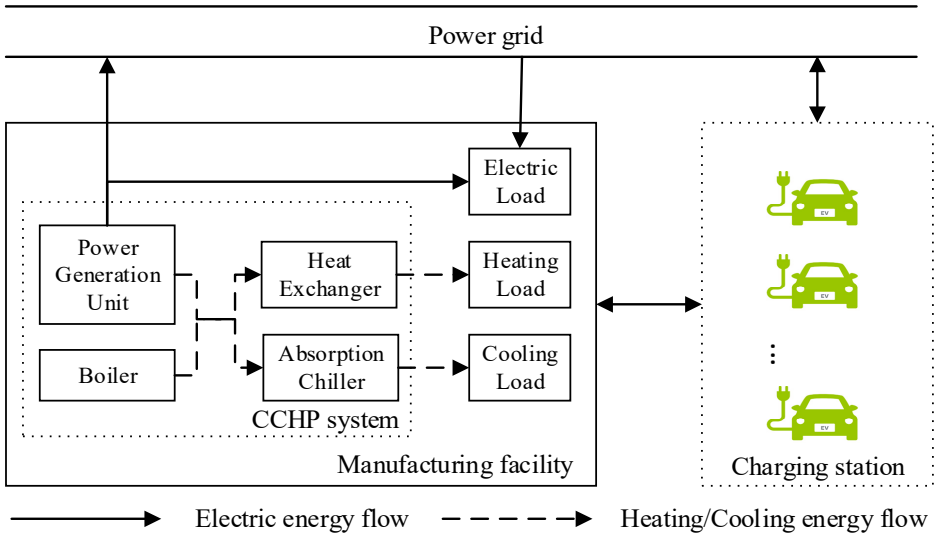

Figure 1. The electric vehicles, power grid, and manufacturing facilities (EPM) Energy Sharing System Structure.

In this paper, the manufacturing facility with a typical serial manufacturing system consisting of N machines and N—1 buffers (as shown in Figure 2) is considered. The electricity load of this production system is supplied by the CCHP system, power grid and EVs. The power grid would provide electricity to the manufacturing system when the electricity generated by the PGU cannot meet the electricity demand; otherwise, the extra power generated by PGU would be sent to the EVs or sold back to the power grid. The electricity demand of EVs is met by the power grid. The electricity of EV batteries also can be sent to the manufacturing facility and the power grid when needed. The heating energy generated from PGU and the auxiliary boiler can be used by the heat exchanger and absorption chiller to satisfy the manufacturing facility's heating load (e.g., hot water and space heating) and cooling load, respectively. In addition, the heating energy generated by the machines' operation in the manufacturing system can affect the facility heating or cooling load.

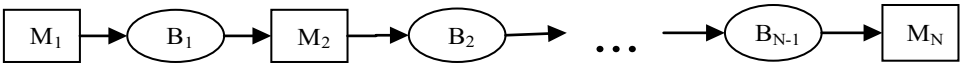

Figure 2. A Typical Serial Manufacturing Production Line with N Machines and N1 Buffers.

As demonstrated in Figures 1 and 2, the objective of this study is to identify the optimal production and energy management strategy for the power grid, EVs, and manufacturing facility under the TOU electricity tariff with a minimal total cost. In the TOU rate, the electricity price during the on-peak period is higher than in the mid-peak and off-peak period. By using the optimal strategy, the proposed system cost, consisting of electricity billing cost, fuel cost, CCHP investment cost, electricity demand charge, and EVs battery use cost, can be minimized under the constraints of manufacturing system characteristics: production target, CCHP system features and EVs characteristics (e.g., EV battery balance and arriving/leaving time). The CDE and PEC of the system optimal strategy are investigated in the case studies, which can provide a better view of environmental and energy performance (i.e., CDE and PEC).

3. Mathematical Modelling

In this section, a MINLP model is formulated to minimize the overall cost by obtaining the optimal strategy for the EPM energy sharing system. The model is established based on a systematic perspective by considering the interrelationships between each component. In addition, the most vital assumptions are fully adopted to assure the accuracy of the calculation results. Moreover, all units are

converted to eliminate the heterogeneity of the model and deliver correct results. The notations of indexes, parameters and variables used in the model are shown in the Appendix A.

3.1. Objective Function

The objective function is formulated in Equation (1). In this equation, *COST* represents the overall cost of the proposed system, which consists of manufacturing facility cost and EV cost. C_F and C_{EVs} denote the costs that are related to manufacturing facility and EVs, respectively.

$$Min \;\; COST = C_F + C_{EVs} \tag{1}$$

3.2. Constraints

3.2.1. Environmental and Energy Evaluation

In this paper, CDE and PEC are adopted to assess the environmental and energy criteria. CDE is the amount of carbon dioxide emissions from fuel consumption of the PGU, boiler and the power grid, and it can be quantified by Equation (2). PEC is identified as the sum amount of site energy consumption and energy losses during the generation, distribution, and transmission of energy, and it can be formulated by Equation (3).

$$CDE = \sum_t \mu^{cchp} \cdot \left(f_t^{pgu} + f_t^{boiler} \right) + \sum_t \mu^{grid} \cdot \left(ef_t^{grid,mf} + \sum_i ef_{i,t}^{grid,ev} \right) \tag{2}$$

$$PEC = \sum_t \sigma^{cchp} \cdot \left(f_t^{pgu} + f_t^{boiler} \right) + \sum_t \sigma^{grid} \cdot \left(ef_t^{grid,mf} + \sum_i ef_{i,t}^{grid,ev} \right) \tag{3}$$

In Equation (2), μ^{cchp} and μ^{grid} are the carbon dioxide emission conversion factors for the CCHP system fuel and the power grid electricity, respectively. In Equation (3), σ^{cchp} and σ^{grid} represent the site-to-primary energy conversion parameters for the CCHP system fuel and the power grid electricity, respectively.

3.2.2. Manufacturing Facility Operation Decision Model

The manufacturing facility cost is described by Equation (4) which includes electricity cost, fuel cost, energy transaction cost, investment cost and electricity demand charge. The first term of the function represents the electricity cost associated with the power grid. The second term indicates the fuel cost consumed by PGU and boiler. The third term shows the energy transaction cost between facility and EVs. The fourth term is the capital cost of each piece of equipment in the CCHP system in one day, where the capital recovery factor can be obtained by Equation (5). The last term represents the electricity demand charge according to the maximum electricity purchased from the power grid during peak periods in the whole production time.

$$\begin{aligned} C_F = & \sum_t \left(P_t^{pur} \cdot ef_t^{grid,mf} - P_t^{sell} \cdot ef_t^{mf,grid} \right) \\ & + \sum_t P_t^f \cdot \left(f_t^{pgu} + f_t^{boiler} \right) \\ & + \sum_{i,t} \left(P_t^{trans} \cdot ef_{i,t}^{ev,mf} - P_t^{trans} \cdot ef_{i,t}^{mf,ev} \right) + A \cdot \left(\sum_q C_q^{cc} \cdot Cap_q \right) / 365 \\ & + R^D \cdot \max_{t \in ONP} \left(ef_t^{grid,mf} / \Delta t \right) \end{aligned} \tag{4}$$

$$A = r(1+r)^y / \left\{ (1+r)^y - 1 \right\} \tag{5}$$

Manufacturing System Constraints

Constraint 6 states that each buffer's occupancy at the beginning of a time interval ranges from zero to its maximum capacity. Equation (7) represents the material balance in the serial manufacturing production line. Constraint 8 is considered to guarantee that the number of produced parts during the planning horizon is no less than the production target. Constraint 9 is to ensure that the electricity from the PGU, power grid and EVs to the manufacturing facility is equal to the electricity demand of the manufacturing system and electricity sent from manufacturing facility to the power grid or EVs. The relationship between the heating from the manufacturing operation and the machine motor efficiency at time t is shown in Equation (10). The heat transferred to the environment correlates with the convective and radiative split ratio of machines, and the instantaneous convective heating and non-instantaneous radiant heating can be calculated by Equations (11) and (12) respectively. In Equation (12), the radiant time series s_t. represents the radiant fraction of the heating which is transferred into the room. Constraint 13 shows the heat transferred from the manufacturing system operation to the surroundings. The constraints expressed in Equations (14) and (15) describe that the space heating or space cooling state depends on the relationship between indoor temperature and outdoor temperature. Equations (16) and (17) show that space heating or space cooling energy are needed to maintain the indoor temperature, except for the manufacturing system operation, respectively. Constraint 18 specifies that additional heating energy supplied from CCHP system is needed when the space heating demand is more than the heat transferred from manufacturing operation. Otherwise, cooling energy is needed when the space heating demand is less than the heat transferred from the manufacturing operation, which is described in Equation (19).

$$0 \le B_{n,t} \le CA_n \cdot n = 1...N-1, \forall t \tag{6}$$

$$B_{n,t} = B_{n,t-1} + x_{n,t-1} \cdot PR_n \cdot EFF_n \cdot \Delta t - x_{n+1,t-1} \cdot PR_{n+1} \cdot EFF_{n+1} \cdot \Delta t \quad n = 1...N-1, \forall t \tag{7}$$

$$\sum_t x_{N,t} \cdot PR_N \cdot EFF_N \cdot \Delta t \ge PT \tag{8}$$

$$ef_t^{pgu} + ef_t^{grid,mf} + \sum_i ef_{i,t}^{ev,mf} = \sum_n x_{n,t} \cdot D_n \cdot \Delta t + ef_t^{mf,grid} + \sum_i ef_{i,t}^{mf,ev} \quad \forall t \tag{9}$$

$$GQ_t = \Delta t \cdot \left[\sum\nolimits_n D_n \cdot x_{n,t} \cdot \left(1 - \eta_n^{station}\right)\right] \forall t \tag{10}$$

$$CQ_t^c = cs \cdot GQ_t \ \forall t \tag{11}$$

$$CQ_t^r = \Delta t \cdot \left[\sum\nolimits_{k=1}^{t} \sum\nolimits_{n=1}^{N} (1 - cs) \cdot s_{t-k+1} \cdot D_n \cdot x_{n,t} \cdot \left(1 - \eta_n^{station}\right)\right] \forall t \tag{12}$$

$$CQ_t = CQ_t^c + CQ_t^r \ \forall t \tag{13}$$

$$Z_t^{sh} = \begin{cases} 1 & if\ Tem_t^{in} \ge Tem_t^{out} \\ 0 & otherwise \end{cases} \quad \forall t \tag{14}$$

$$Z_t^{sc} = \begin{cases} 1 & if\ Tem_t^{in} < Tem_t^{out} \\ 0 & otherwise \end{cases} \quad \forall t \tag{15}$$

$$Q_t^{sh} = Z_t^{sh} \cdot c \cdot p \cdot V \cdot \left(Tem_t^{in} - Tem_t^{out}\right) \forall t \tag{16}$$

$$Q_t^{sc} = Z_t^{sc} \cdot c \cdot p \cdot V \cdot \left(Tem_t^{out} - Tem_t^{in}\right) \forall t \tag{17}$$

$$Z_t^{heat} = \begin{cases} 1 & if\ Q_t^{sh} \geq CQ_t \\ 0 & otherwise \end{cases} \quad \forall t \tag{18}$$

$$Z_t^{cool} = \begin{cases} 1 & if\ 0 < Q_t^{sh} < CQ_t \\ 0 & otherwise \end{cases} \quad \forall t \tag{19}$$

Constraints for CCHP System

The energy generated from the PGU and boiler is restricted by their capacities, as shown in Equations (20) and (21). Equation (22) describes that the electric energy by the PGU is restricted by the fuel consumption and electricity conversion efficiency. Constraint 23 is to guarantee that the heating energy generated by the PGU and boiler are consumed by heat exchanger and absorption chiller. Equation (24) denotes that the manufacturing facility heating demand, which consists of hot water, space heating and the heat generated by manufacturing operations, can be satisfied by the heat exchanger in CCHP system. The constraint expressed in Equation (25) indicates that the absorption chiller in CCHP system can provide cooling energy to meet the manufacturing facility cooling demand for space cooling or space heating considering the effect of manufacturing operation.

$$f_t^{pgu} \leq Cap_{pgu}\ \forall t \tag{20}$$

$$f_t^{boiler} \leq Cap_{boiler}\ \forall t \tag{21}$$

$$f_t^{pgu} = \begin{cases} a \cdot ef_t^{pgu} + b\ if\ ef_t^{pgu} > 0 \\ 0\ if\ ef_t^{pgu} = 0 \end{cases} \quad \forall t \tag{22}$$

$$q_t^{hc} + q_t^{cc} \leq \eta^{rec} \cdot f_t^{pgu} + \eta^{bo} \cdot f_t^{boiler}\ \forall t \tag{23}$$

$$\eta^{hc} \cdot q_t^{hc} = Qh_t^{hw} + Z_t^{heat} \cdot \left(Q_t^{sh} - CQ_t\right) \forall t \tag{24}$$

$$\eta^{cc} \cdot q_t^{cc} = Z_t^{sc} \cdot \left(Q_t^{sc} + CQ_t\right) + Z_t^{cool} \cdot \left(CQ_t - Q_t^{sh}\right) \forall t \tag{25}$$

3.2.3. Electric Vehicles Operation Decision Model

During the EV parking time, Equation (26) shows that the energy cost of all the EVs is associated with the electricity cost from power grid, electricity energy transaction cost with the manufacturing facility and EV battery use cost. Equations (27) and (28) represent the EV battery charging and discharging balance, respectively. The constraint expressed in Equation (29) indicates that EVs cannot be in charging and discharging states at the same time. Equations (30) and (31) ensure that the EV battery charging and discharging electricity is restricted by their maximal and minimal charging and discharging rate, respectively. Constraints 32–33 denote the energy storage balance of the EV battery. Equation (34) enforces that the electricity stored in the EV battery is limited by their upper and lower bound. Constraint 35 states that the EV owners' desired battery electricity levels are achieved when the EVs leave the parking area.

$$\begin{aligned} C_{EVs} = & \sum_{i,t}\left(P_t^{pur} \cdot ef_{i,t}^{grid,ev} - P_t^{sell} \cdot ef_{i,t}^{ev,grid}\right) \\ & + \sum_{i,t}\left(P_t^{trans} \cdot ef_{i,t}^{mf,ev} - P_t^{trans} \cdot ef_{i,t}^{ev,mf}\right) + P^{ev} \\ & \cdot \left(\sum_{i,t}\left(ef_{i,t}^{ev,ch} + ef_{i,t}^{ev,disch}\right)\right) / 2 \cdot Cap_{ev} \end{aligned} \tag{26}$$

$$ef_{i,t}^{grid,ev} + ef_{i,t}^{mf,ev} = \eta^{ev,ch} \cdot ef_{i,t}^{ev,ch}\ \forall i, t \in \left[T_i^{arv}, T_i^{dep}\right] \tag{27}$$

$$ef_{i,t}^{ev,grid} + ef_{i,t}^{ev,mf} = \eta^{ev,disch} \cdot ef_{i,t}^{ev,disch}\ \forall i, t \in \left[T_i^{arv}, T_i^{dep}\right] \tag{28}$$

$$xc_{i,t} + xd_{i,t} \le 1 \ \forall i, t \in \left[T_i^{arv}, T_i^{dep}\right] \tag{29}$$

$$S_i{\cdot}\alpha_i^{cmin}{\cdot}xc_{i,t} \le ef_{i,t}^{ev,ch} \le S_i{\cdot}\alpha_i^{cmax}{\cdot}xc_{i,t} \ \forall i, t \in \left[T_i^{arv}, T_i^{dep}\right] \tag{30}$$

$$S_i{\cdot}\alpha_i^{dmin}{\cdot}xd_{i,t} \le ef_{i,t}^{ev,disch} \le S_i{\cdot}\alpha_i^{dmax}{\cdot}xd_{i,t} \ \forall i, t \in \left[T_i^{arv}, T_i^{dep}\right] \tag{31}$$

$$es_{i,t} = es_{i,t-1} + ef_{i,t}^{ev,ch} - ef_{i,t}^{ev,disch} \ \forall i, t \in \left[T_i^{arv}, T_i^{dep}\right] \tag{32}$$

$$es_{i,t} = S_i{\cdot}SOC_i^{arv} + ef_{i,t}^{ev,ch} - ef_{i,t}^{ev,disch} \ \forall i, t = T_i^{arv} \tag{33}$$

$$S_i{\cdot}SOC_i^{min} \le es_{i,t} \le S_i{\cdot}SOC_i^{max} \ \forall i, t \in \left[T_i^{arv}, T_i^{dep}\right] \tag{34}$$

$$es_{i,t} \ge S_i{\cdot}SOC_i^{dep} \ \forall i, t = T_i^{dep} \tag{35}$$

4. Solution Approach

The MINLP model is established for the optimization problem of the collaborative energy sharing among the manufacturing facility, EVs and the power grid. The mathematic model is non-convex due to the objective function 1 and Constraints 14, 15, 18, 19, 22. Moreover, the binary decision variables also increase the complexity of the solution. The PSO algorithm provided a powerful tool to solve the problems of non-convex and discrete decision variables [45]. The PSO is an evolutionary method based on the stochastic optimization technique, and is inspired by the social behavior of animals (birds) [46]. In the PSO algorithm, each particle, characterized by position and velocity, represents a feasible solution, which moves according to its own previous best position and the swarm's previous best position. Particles in swarms have fitness values, which are evaluated by the fitness function. Particles, like birds, fly through the search space towards global optimal solutions. Owing to its good performance with fast convergence rates and ease of implementation, the PSO algorithm has been successfully used to solve non-convex problems in wide areas such as power generation systems dispatch [47], intermodal transportation [48], and optimal power flow problem in power systems [21].

Therefore, the PSO algorithm is adopted to obtain the optimal solutions of manufacturing schedule, EVs, and power grid in this study. In the PSO algorithm, each candidate solution of the manufacturing system production, CCHP operational strategy and EV charging/discharging schedule is considered as a particle in the swarm. For a swarm of population size S and iteration size K, the D-dimensional particle, $\left(L_{d,s}^k, v_{d,s}^k\right)$, is described as the position and velocity of each particle, where $k = 1, \ldots, K, d = 1, \ldots, D$ and $s = 1, \ldots, S$. The initial solution of all the decision variables is randomly generated within their ranges. The evolution of position and velocity can be guided by following formulae in the searching space over iterations.

$$v_{d,s}^{k+1} = w{\cdot}v_{d,s}^k + c_1{\cdot}r_1{\cdot}\left(pbest_{d,s}^k - L_{d,s}^k\right) + c_2{\cdot}r_2{\cdot}\left(gbest_s^k - L_{d,s}^k\right) \forall k, d, s \tag{36}$$

$$L_{d,s}^{k+1} = L_{d,s}^k + v_{d,s}^{k+1} \ \forall k, d, s \tag{37}$$

Term k and $k+1$ denote the k^{th} and $(k+1)^{th}$ iteration, respectively. In the k^{th} iteration, $pbest_{d,s}^k$ shows the s^{th} particle's best solution and $gbest_s^k$ represents the global best solution obtained by the entire swarm. In Equation (37), the second and third term are stochastic terms. In addition, r_1, r_2 are random numbers generated in the range of [0,1], and are intended to simulate the slight unpredictable component of natural swarm behavior. The positive learning factors c_1, c_2 determine how much the particle is influenced by *pbest* and *gbest*, respectively. Moreover, it is suggested by the PSO developers that $c_1 = c_2 = 2$ is a good choice, and able to render the stochastic terms a mean of 1 to make the particles "overfly" the *pbest* and *gbest* around half of the time [49,50].

In the PSO algorithm, balancing the local and global search throughout the course of run is critical, which is controlled by the inertia weight w. A large value of w represents better global search

ability, while a small w value means better local search ability. The search process is non-linear and complicated, thus a linear decreasing function from inertia PSO is used to dynamically adjust the search ability in the iterative process [51,52]. As shown in Equation (38), w changes from the maximum inertia weight w_{max} to the minimum inertia weight w_{min} through the course of a PSO run, which means a greater global search ability at the beginning and a greater local search ability near the end. Term w linearly decreasing from 0.9 to 0.4 is proved to be capable of greatly improving the performance of PSO on the benchmark problems [50]. Therefore, w_{max} and w_{min} are set to be 0.9 and 0.4, respectively.

$$w = w_{max} - [(w_{max} - w_{min})/K] \cdot k \ \forall k \tag{38}$$

Since both position and velocity of particles are renovated using real numbers in Equations (36) and (37), further steps, as shown in (39) and (40), are needed to restrict the velocity and position of the machine state, EV charging state, and EV discharging state in the sets {−1,0,1} and {0,1}, respectively.

$$v_{d,s}^{k+1} = \begin{cases} -1 & if \quad v_{d,s}^{k+1} < -0.5 \\ 0 & if \quad -0.5 \le v_{d,s}^{k+1} \le 0.5 \\ 1 & if \quad v_{d,s}^{k+1} > 0.5 \end{cases} \quad \forall k, d, s \tag{39}$$

$$L_{d,s}^{k+1} = \begin{cases} 0 & if \quad L_{d,s}^{k} + v_{d,s}^{k+1} \le 0 \\ 1 & if \quad L_{d,s}^{k} + v_{d,s}^{k+1} \ge 1 \end{cases} \quad \forall k, d, s \tag{40}$$

The fitness function of each particle can be evaluated by Equation (41) with the Constraints 6, 8, 20, 21, 23, 29, 30, 31, 34 and 35 integrated as penalty terms, where $A_1, A_2, A_3, A_4, A_5, A_6, A_7, A_8, A_9, A_{10}$ are ten large real numbers.

$$\begin{aligned} & COST \\ & + A_1 \cdot min\left[(CA_n - B_{n,t}, 0)^2 + min(B_{n,t}, 0)^2 \right] \\ & + A_2 \cdot \left(\sum_t x_{N,t} \cdot PR_N \cdot EFF_N \cdot \Delta t - PT, 0 \right)^2 \\ & + A_3 \cdot min\left(Cap_{pgu} - f_t^{pgu}, 0 \right)^2 + A_4 \cdot min\left(Cap_{boiler} - f_t^{boiler}, 0 \right)^2 \\ & + A_5 \cdot min\left[\eta^{rec} \cdot f_t^{pgu} + \eta^{bo} \cdot f_t^{boiler} - \left(q_t^{hc} + q_t^{cc} \right), 0 \right]^2 \\ & + A_6 \cdot min[1 - (xc_{i,t} + xd_{i,t}), 0]^2 \\ & + A_7 \cdot \left[min\left(S_i \cdot \alpha_i^{cmax} \cdot xc_{i,t} - ef_{i,t}^{ev,ch}, 0 \right)^2 \right. \\ & \qquad \left. + min\left(ef_{i,t}^{ev,ch} - S_i \cdot \alpha_i^{cmin} \cdot xc_{i,t}, 0 \right)^2 \right] \\ & + A_8 \cdot \left[min\left(S_i \cdot \alpha_i^{dmax} \cdot xd_{i,t} - ef_{i,t}^{ev,disch}, 0 \right)^2 \right. \\ & \qquad \left. + min\left(ef_{i,t}^{ev,disch} - S_i \cdot \alpha_i^{dmin} \cdot xd_{i,t}, 0 \right)^2 \right] \\ & + A_9 \cdot \left[min\left(S_i \cdot SOC_i^{max} - es_{i,t}, 0 \right)^2 + min\left(es_{i,t} - S_i \cdot SOC_i^{min}, 0 \right)^2 \right] \\ & + A_{10} \cdot \left(es_{i,t} - S_i \cdot SOC_i^{dep}, 0 \right)^2 \\ & \forall i, t \end{aligned} \tag{41}$$

The learning factors c_1 and c_2 are usually assumed as $c_1 = c_2 = 2$; the w_{max} and w_{min} are set to be 0.9 and 0.4, respectively [53]. There exists a tradeoff between computational cost and accuracy of the optimal solution in the PSO algorithm [54]. The parameter combinations of S and K have to be tested and selected to balance the computational efficiency and solution quality. The PSO implementation is concisely depicted in Figure 3. In addition, the relative standard deviation (RSD) is used to help determine the optimal result. First, the PSO-based solution algorithm is run for multiple trials, usually more than 100 times, to obtain the optimal result. Next, the RSD of the total cost values

are calculated for all trials. If the RSD is smaller than 1%, we conclude that the obtained results are stable; otherwise, more trials will be conducted until the RSD is less than 1%. Then, we use the lowest total cost of all trials as the optimal result. In this way, we can avoid the result falling into a local optimum.

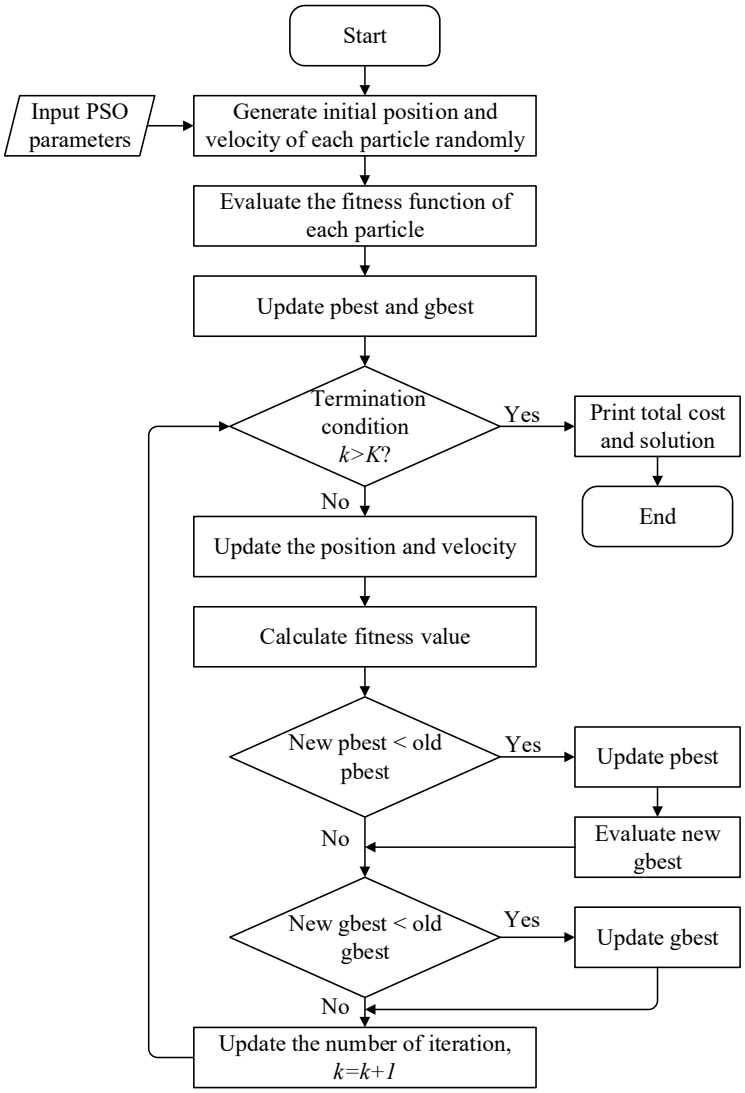

Figure 3. The Flowchart of the Optimization Process using the particle swarm optimization (PSO) Algorithm.

5. Case Studies

To evaluate the economic criterion of the proposed system using the formulated MINLP model, cases are investigated for the EPM system located in San Francisco, U.S. The manufacturing system is assumed to be in a one-story and one-thermal-zone facility, whose floor area is 20 x 20 m and the height is 10 m. The specific heat capacity and density of air are 0.00028 kWh/kg and 1.29 kg/m^3, respectively. Two production schedules, one working shift (8 h) and two working shifts (16 h), are considered. The TOU electricity tariff can charge different prices at three periods (i.e., on-peak, mid-peak, off-peak) in one day. In order to analyze the EPM system under the TOU electricity tariff, a winter day and a summer day for one-shift/two-shift production are conducted in this study.

In this section, the manufacturing facility, including a five-machine-four-buffer serial manufacturing production line, is adopted. Each machine parameter, e.g., production rate and rated power, is displayed in Table 1. The parameters of each buffer, i.e., initial contents and capacities,

are also presented in Table 1. The radiant and convective sections of the machines are assumed to be 0.3 and 0.7, respectively [55]. The radiant time series are assumed as shown in Figure 4 [56].

Table 1. Machine and Buffers Parameters.

Machine Parameters					Basic Setting of Buffers		
Machine	**Production Rate (unit/h)**	**Power (Kw)**	**Efficiency**	**Motor Efficiency**	**Buffer**	**Initial Contents**	**Capacity**
M1	40	26	90%	0.85	B1	90	180
M2	40	30	90%	0.85	B2	80	160
M3	40	42	90%	0.80	B3	75	150
M4	40	32	90%	0.85	B4	80	180
M5	40	40	90%	0.80	-	-	-

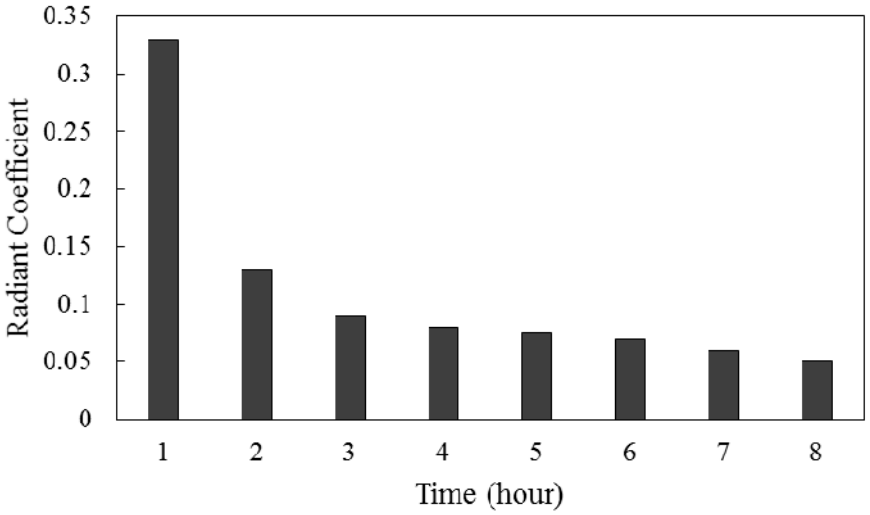

Figure 4. Radiant Time Series Coefficients.

According to the literature [57], the capacities and unit prices of the CCHP system equipment are assumed as shown in Table 2. Other parameters related to the manufacturing facility are shown in Table 3 [58]. The electricity transaction price is assumed to be a constant and is set to be 0.00367 USD/kWh [58,59]. For the facility, it is expected that the parking area has a maximum capacity of 100 vehicles and 30% of the parked vehicles are EVs. Moreover, it is assumed that there are 30 EVs in the parking lot and each EV has a battery capacity of 30 kWh with 95% charging and discharging efficiencies. The EVs arrive at the parking lot with 30% battery charged and prefer to leave with 80% charged battery [7]. In addition, all the workers are assumed to arrive and leave on time. The minimal and maximal charging/discharging rates for EVs are set to be 2 kW and 20 kW, respectively. The depreciation cost of one EV's charging cycle (i.e., charge EV's battery from empty to fully charged, then discharge it to empty) is assumed to be 10 $US.

Table 2. Parameters of CCHP System Equipment.

	PGU	**Boiler**	**Heat Exchanger**	**Absorption Chiller**
Capacity (kW)	900	1200	300	600
Unit price (USD/kW)	1046	46	30	185

Table 3. The Manufacturing Facility Related Parameters.

Parameter	Value	Unit
a	2.97	-
b	11.66	-
η^{rec}	0.51	-
η^{bo}	0.9	-
η^{hc}	0.85	-
η^{cc}	0.7	-
r	0.03	-
y	20	-
P_t^f	0.027	USD/kWh
P_t^{sell}	0.00367	USD/kWh
μ^{cchp}	0.000184	tons/kWh
μ^{grid}	0.000554	tons/kWh
σ^{cchp}	1.047	-
σ^{grid}	3.336	-

In order to validate the economic advantage of the proposed EPM energy sharing system, a baseline case is conducted in this section. In the baseline case, no interrelation exists between EVs and the manufacturing facility. In addition, the CCHP system is not used for the manufacturing facility. The manufacturing system electricity demand is met by the power grid, while the heating and cooling demand are supplied by boiler. The power grid supplies electricity to each EV. Moreover, the facility and EVs cannot sell electricity to the power grid. The baseline case parameters are the same as the proposed system.

The optimal problems are solved by the PSO algorithm. In order to balance the optimal solution and computational cost, the reasonable population size and maximum number of iterations are set as $S = 2000$ and $K = 200$ by trying different parameter combinations. The proposed MINLP model and PSO algorithm are coded in MATLAB on a desktop computer equipped with an Intel(R) Core (TM) i5-8265U CPU @1.60GHz processor, and 8GB memory.

5.1. One-Shift Production Schedule

In the one-shift production horizon, the period is from 9:00 a.m. to 5:00 p.m. The time period is divided into 32 15-min intervals since the electricity demand is charged over each 15-min interval. The target PT for the one-shift production is set at 252. The demand charge is based on the maximal electricity consumption during on-peak period.

5.1.1. Winter Days for One-Shift Production

In this section, the TOU electricity rate from the PGE company [60] as shown in Table 4 is utilized as the electricity price from the power grid. In this winter day for one-shift production schedule case, the 8 h are all during the on-peak period.

Table 4. The winter electric rate under time-of-use (TOU) tariff from PGE for one-shift production.

Months	On-Peak	Electric Charge (USD/kWh)	Demand Charge (USD/kW)
		On-Peak	On-Peak
Nov–Apr	8:30–21:30	0.10171	14.84

From 9:00 a.m. to 5:00 p.m. in the winter day, the outdoor temperature [61] and the expected indoor temperature of the manufacturing facility in San Francisco are shown in Figure 5.

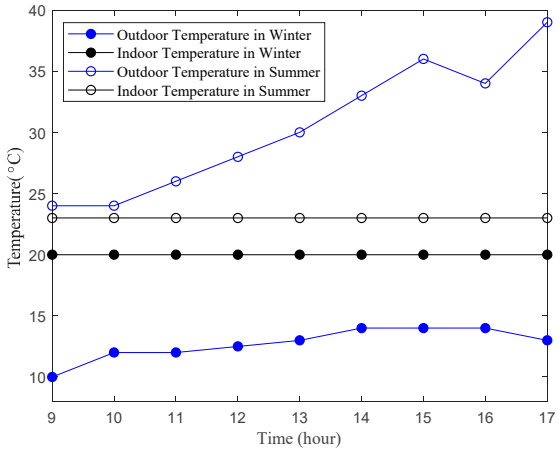

Figure 5. The outdoor and expected Indoor Temperature for one-shift production.

The hot water demand of facility is calculated as shown in Figure 6a by considering the hot water set point as 60 °C, the outdoor temperature and the industrial facility size [62].

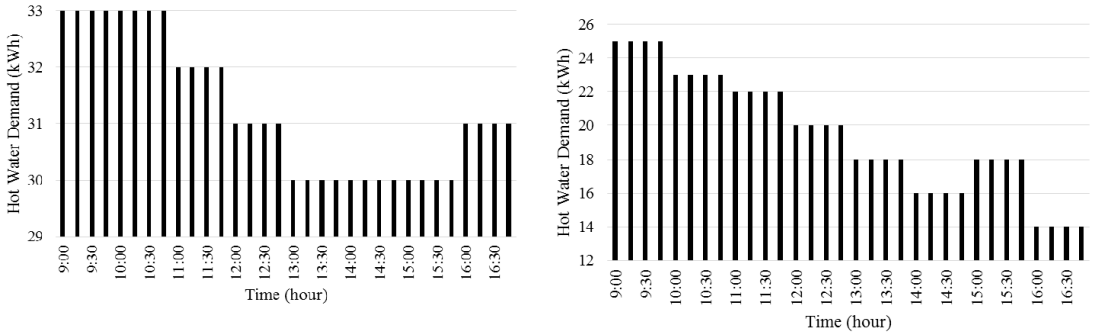

(**a**) Winter day (**b**) Summer day

Figure 6. The 15-min basis hot water demand (kWh) of the manufacturing facility for one-shift production.

The optimal strategy of the proposed system and baseline case in the winter day for one-shift production are obtained by adopting the PSO algorithm to solve the formulated MINLP model. The PSO algorithm is executed with 100 independent runs, and the averaged time as well as the statistical results are provided in Table 5. The calculated RSD is quite small, which means the fitting value of the PSO algorithm is stable at the parameter combinations. The solutions that result in the least total cost are used as the optimal solutions for the EPM system and baseline case.

Table 5. The statistical results of the EPM system and baseline case solved by PSO Algorithm with 10 trial runs on the winter day for one-shift production.

	Avg. Time (s)	Min (USD)	Mean (USD)	Max (USD)	RSD (%)
Optimized case	460.71	2417.37	2446.74	2470.47	0.82
Baseline case	260.14	3133.11	3151.70	3189.59	0.64

By using the PSO algorithm, the optimal solution of the EPM system is obtained. The optimal production schedule for the manufacturing system is shown in Figure 7a, and the vertical axis and horizontal axis present machines and time, respectively. The electricity supply and demand curve in the winter day for the one-shift production are illustrated in Figure 7b, which shows the electricity balance in EPM energy sharing system. The electricity flows among the power grid, manufacturing facility and EVs are shown in Figure 7c. Note that in Figure 7b,c, the negative values denote the reverse

flow of electricity. For example, electricity is sold back to the power grid at 16:15 as shown in Figure 7b, and the power is fed back to the power grid from manufacturing facility at 9:15 in Figure 7c.

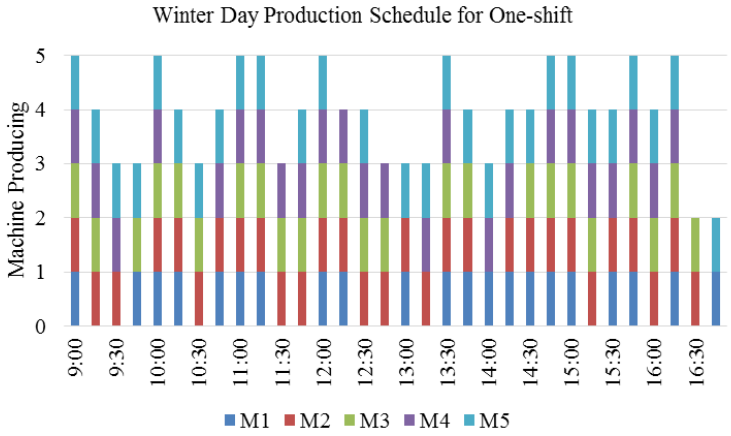

(**a**) The optimal production schedule for the manufacturing system.

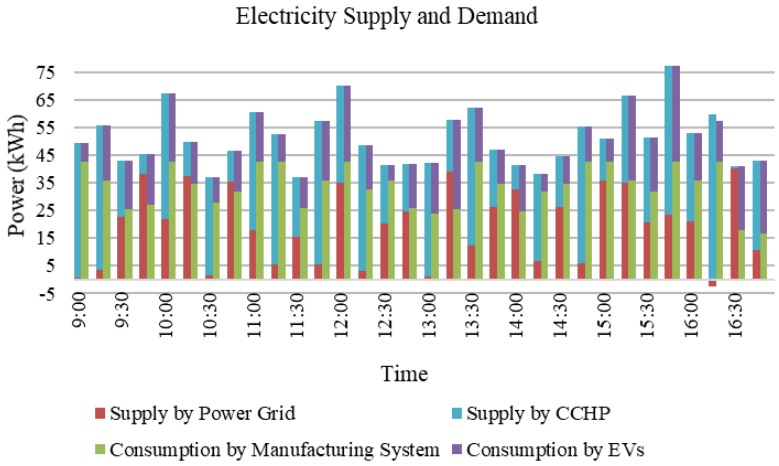

(**b**) The electricity supply and demand curve.

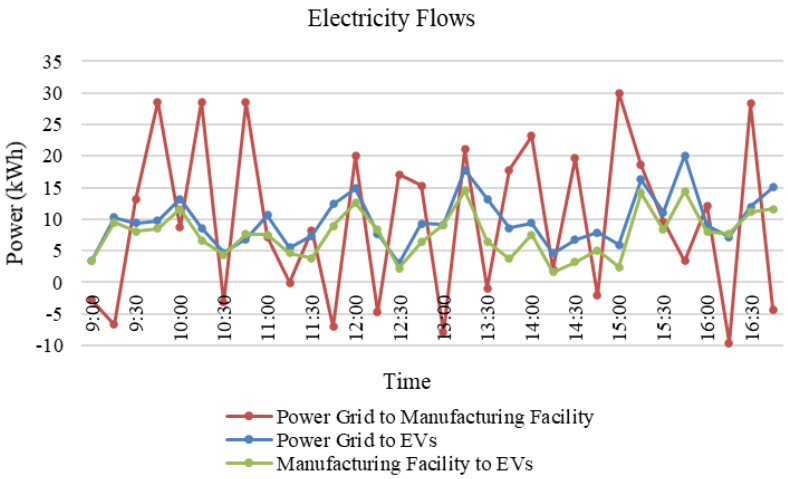

(**c**) the Electricity Flows.

Figure 7. The optimal solution of the EPM system on the winter day for one-shift production.

The economic performance comparison between the proposed EPM system and the baseline case under the TOU tariff in the winter day for one-shift is presented in Table 6. Table 6 demonstrates that the overall cost obtained by adopting the EPM energy sharing system is 22.84% lower than the baseline case. The largest portion of the system cost is from the demand charge, which accounts for 73.67% of the total cost. In addition, the results indicate that the demand charge in the EPM energy sharing system is 33.22% less than the baseline case. The main reason is that the electricity peak demand is reduced by using EVs as the energy storage. Moreover, the EV battery depreciation cost in the system is more than that of the baseline case, which indicates that the EV battery charging/discharging frequency is increased in the EPM energy sharing system.

Table 6. The cost (USD) comparison between the optimized case and baseline case on the winter day for one-shift production.

	Total Cost	Electricity		Fuel	Equipment		EVs Battery	Demand Charge
		Facility	EVs		CCHP	Boiler		
Optimized case	2417.37	45.18	44.93	162.49	205.62	-	178.35	1780.8
Baseline case	3133.11	134.47	58.73	234.17	-	39.04	91.43	2666.71
Cost saving	22.84%							

To better assess the benefits of the proposed system, the environmental and energy performance of the optimal strategy are investigated. By adopting the optimal solution, the *CDE* and *PEC* results for the EPM energy sharing system and baseline case are shown in Table 7. It is demonstrated that the system can achieve 39.62% CDE reduction and 39.75% PEC saving compared with the baseline case, respectively. In addition, CDE and PEC of the power grid are reduced by 53.33% and 52.84% compared with the baseline case. Furthermore, 30.63% and 30.61% reduction can be achieved in CDE and PEC of the equipment, respectively.

Table 7. The *CDE* and *PEC* comparison on the winter day for one-shift production.

	CDE (Tons)			*PEC* (kWh)		
	Total	Equipment	Power Grid	Total	Equipment	Power Grid
Optimized case	1.60	1.11	0.49	9289.26	6301.15	2988.11
Baseline case	2.65	1.60	1.05	15,417.22	9080.48	6336.74
Reduction	39.62%	30.63%	53.33%	39.75%	30.61%	52.84%

5.1.2. Summer Days for One-Shift Production

The differences between winter days and summer days for one-shift production lie in the electricity price, outdoor temperature, hot water demand, and demand charge rate. In this case, the TOU rate from the PGE company [60] is applied for the electricity price from the power grid in the summer day (shown in Table 8). During the 8 h in the summer day, the outdoor temperature [61] and expected indoor temperature for the facility are shown in Figure 5. The hot water demand of the manufacturing facility is obtained as shown in Figure 6b when the hot water set point is 60 °C [62].

Table 8. The summer electric rate under the TOU tariff from PGE for one-shift production.

Months	On-Peak	Mid-Peak	Electric Rate (USD/kWh)		Demand Charge (USD/kW)
			On-Peak	Mid-Peak	On-Peak
May–Oct	12–18	8:30–12; 18–21:30	0.14944	0.10739	32.19

The setup for baseline case in summer days for one-shift production follows the same logic as the one-shift production in winter days. The optimized production schedule for the manufacturing system is illustrated in Figure 8a. The electricity equilibrium of the EPM system is presented in Figure 8b. The electricity flows among the power grid, manufacturing facility and EVs are shown

in Figure 8c. According to Figure 8c, during on-peak period (i.e., 12:00-17:00) with higher electricity prices, electricity is sold back from the manufacturing facility to the power grid at 12:00, 12:30, 13:15, 13:30, 14:45 and 16:00.

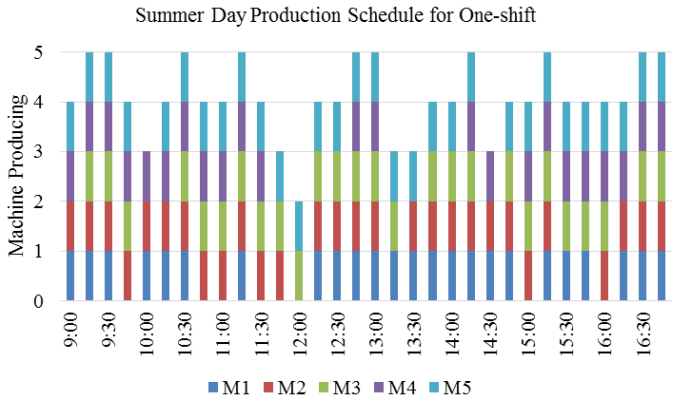

(**a**) the optimal production schedule for the manufacturing system.

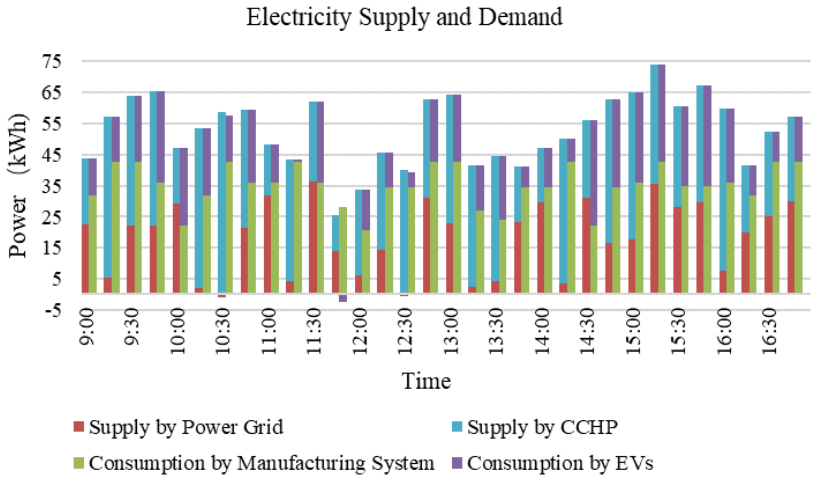

(**b**) The electricity supply and demand curve.

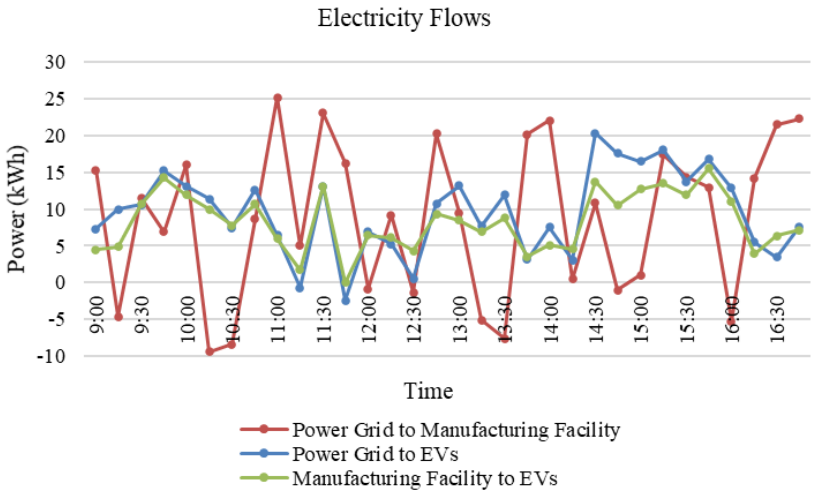

(**c**) The electricity flows.

Figure 8. The optimized solution of the EPM System on the summer day for one-shift production.

In the summer day for one-shift production, the cost breakdowns of the proposed EPM energy sharing system and the baseline case are obtained as shown in Table 9. The overall cost is reduced by 34.81% compared with the baseline case. In addition, the purchased electricity from the power grid is 50.70% less than the baseline case. Compared with winter days scenarios, the cost saving is more significant for one-shift production in the summer day. This is probably because the cost for cooling energy demand can be saved when production is adjusted to the off-peak hours during summer day.

Table 9. The cost (USD) comparison between the optimized case and baseline case on the summer day for one-shift production.

	Total Cost	Electricity		Fuel	Equipment		EVs Battery	Demand Charge
		Facility	EVs		CCHP	Boiler		
Optimized case	3883.29	58.39	62.33	214.16	205.62	-	190.89	3151.89
Baseline case	5957.17	168.49	76.40	200.98	-	39.04	90.05	5472.22
Cost saving	34.81%							

The CDE and PEC of the presented EPM energy sharing system and baseline case are shown in Table 10 when the optimal strategy is adopted. Compared with the baseline case, the system can achieve 18.00% CDE reduction and 18.53% PEC saving. It is interesting to observe that the equipment caused CDE and PEC between the optimized case and baseline case are quite close in summer scenarios, while these values in the optimized case decreases considerably in the winter. This indicates that more energy is consumed for cooling in summer than the energy for heating in winter, since machines can off-set part of the heating energy.

Table 10. The *CDE* and *PEC* comparison on the summer day for one-shift Production.

	CDE (tons)			*PEC* (kWh)		
	Total	Equipment	Power Grid	Total	Equipment	Power Grid
Optimized case	1.96	1.46	0.51	11,345.80	8304.64	3041.16
Baseline case	2.39	1.37	1.02	13,925.65	7793.72	6131.93
Reduction	18.00%	−6.57%	50%	18.53%	−6.56%	50.40%

5.2. Two-Shift Production Schedule

The two-shift production horizon consists of two periods. The first shift takes place from 6:00 a.m. to 2:00 p.m. and the second shift is from 2:00 p.m. to 10:00 p.m. The production target of each shift is set at 252. In addition, the electricity demand charge is the fee of the highest electricity demand during on-peak time in the whole day.

5.2.1. Winter Days for Two-Shift Production

For two-shift production, the electricity rates during on-peak/off-peak periods and electricity demand charge rate are listed in Table 11 for the winter day [61].

Table 11. The Winter Electric Rate under the TOU Tariff from PGE for Two-Shift Production.

Months	On-Peak	Off-Peak	Electric Charge (USD/kWh)		Demand Charge (USD/kW)
			On-Peak	Off-Peak	On-Peak
Nov–Apr	8:30–21:30	21:30–8:30	0.10171	0.08704	14.84

From 6:00 a.m. to 10:00 p.m. in the winter day, the outdoor temperature [61] and expected indoor temperature for the manufacturing facility in San Francisco are shown in Figure 9. The hot water demand of the industrial facility is calculated, as shown in Figure 10a, by considering the hot water set point as 60 °C, the outdoor temperature, and the industrial facility size [62].

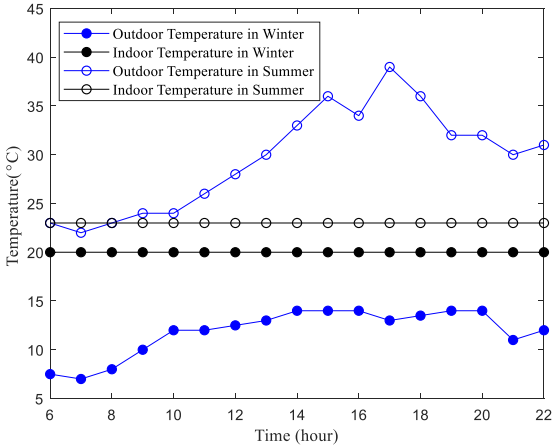

Figure 9. The Outdoor and Expected Indoor Temperature for Two-Shift Production.

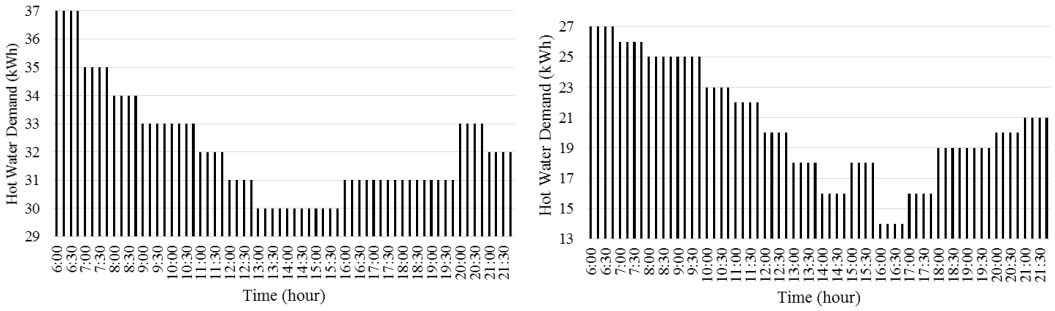

(**a**) in the Winter Day (**b**) in the Summer Day

Figure 10. The 15-min basis Hot Water Demand (kWh) of the Manufacturing Facility for Two-Shift Production.

The optimal production schedule for this manufacturing system is presented in Figure 11a, and Figure 11b shows the electricity supply and demand curve. It can be observed from Figure 11b that electricity is sold back to power grid at some time intervals (e.g., 8:45 and 20:00) during the on-peak period (i.e., 8:30-21:30), while no electricity is transferred to the power grid during the off-peak period. The electricity exchange among EVs, the manufacturing facility and the power grid is illustrated in Figure 11c, which also shows that the electricity can be supplied from EVs to manufacturing facility in the on-peak time (e.g., 11:00 and 19:00).

In the winter day for two-shift production, the cost breakdown of the overall EPM energy sharing system and baseline case are presented in Table 12. It can be noted that the proposed system total cost can achieve 16.73% reduction, compared to the baseline case. The largest share of total cost is the demand charge, which accounts for 57.89% of the total cost. The fuel cost is the second largest cost component with 16.80%. Compared with the baseline case, the purchased electricity cost contributes to the greatest saving with 56.89%. However, the equipment cost exhibits the largest increase. In addition, Tables 6 and 12 indicate that the two-shift production optimal strategy cost saving is smaller than one-shift production optimal solution cost reduction in the winter day. This is mainly because the fuel consumption is actually higher in the optimized case, while the fuel cost is lower than baseline case in the one-shift scenario in winter days.

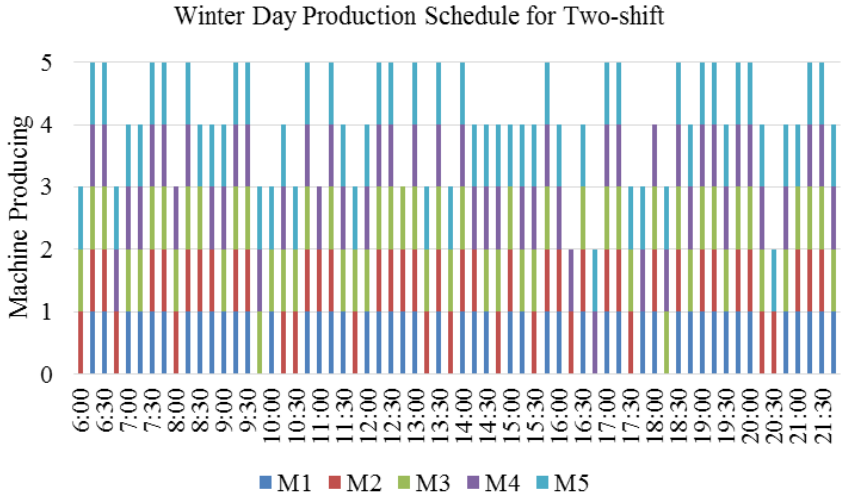

(a) The Optimal Production Schedule for Manufacturing System.

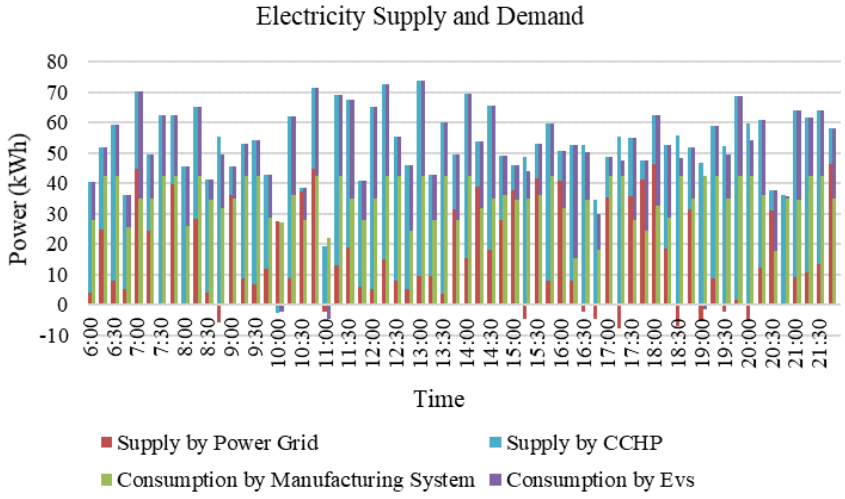

(b) The Electricity Supply and Demand Curve.

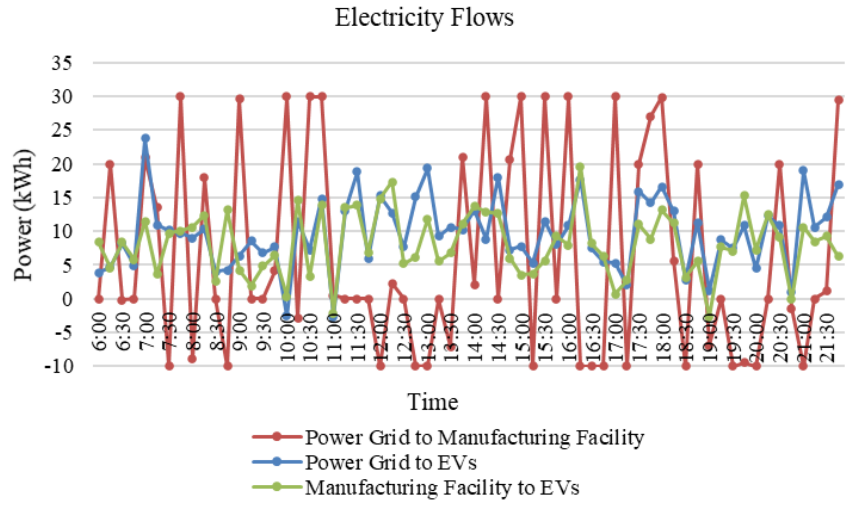

(c) the Electricity Flows.

Figure 11. The Optimal Solution of EPM System in the Winter Day for Two-Shift Production.

Table 12. The Cost (USD) Components Between the Optimized Case and Baseline Case on the Winter Day for Two-Shift Production.

	Total Cost	Electricity		Fuel	Equipment		EVs Battery	Demand Charge
		Facility	EVs		CCHP	Boiler		
Optimized case	3076.11	63.59	94.67	516.73	205.62	-	414.70	1780.8
Baseline case	3694.17	265.14	110.7	437.96	-	39.04	177.25	2841.31
Cost saving	16.73%							

Table 13 shows that the system in the winter day for two-shift achieves about 13.16% CDE reduction and 14.12% PEC saving than the baseline case, respectively. The CDE and PEC of the equipment in the system are 18.12% and 17.99% larger than the baseline case, respectively; while the power grid CDE and PEC are 57.25% and 57.13% lower than the baseline case, respectively.

Table 13. The *CDE* and *PEC* Comparison on the Winter Days for Two-Shift Production.

	CDE (tons)			*PEC* (kWh)		
	Total	Equipment	Power Grid	Total	Equipment	Power Grid
Optimized case	4.42	3.52	0.902	25,471.58	20,037.50	5434.08
Baseline case	5.09	2.98	2.11	29,658.42	16,983.09	12,675.33
Reduction	13.16%	−18.12%	57.25%	14.12%	−17.99%	57.13%

5.2.2. Summer Days for Two-Shift Production

The differences between winter days and summer days for the two-shift production are also reflected in electricity price, outdoor temperature, hot water demand, and demand charge rate. For the two-shift production, the TOU price for on-peak/off-peak periods and electricity demand charge rate are given in Table 14 [60]. During the 16 h in the summer day, the outdoor temperature [61] and expected indoor temperature for the manufacturing facility in San Francisco are shown in Figure 9. The hot water demand is shown as Figure 10b by considering the hot water set point as 60 °C, the outdoor temperature, and the industrial facility size [62].

Table 14. The Summer Electric Rate under TOU Tariff from PGE for Two-Shift Production.

May-Oct	On-Peak	Mid-Peak	Off-Peak
Time (hour)	12–18	8:30–12; 18–21:30	21:30–8:30
Electric charge (USD/kWh)	0.14944	0.10739	0.08036
Demand charge (USD/kW)	32.19	-	-

The optimal production schedule of the manufacturing system is given in Figure 12a. The electricity balance of the EPM system is illustrated in Figure 12b,c, representing the electricity exchange among EVs, the power grid, and the manufacturing facility. According to Figure 12b,c, electricity can be sold back to the power grid and electricity can be transferred from EVs to manufacturing facility or power grid, due to a higher electric rate during the on-peak period (i.e., 12:00–18:00) and mid-peak (e.g., 8:30–12:00).

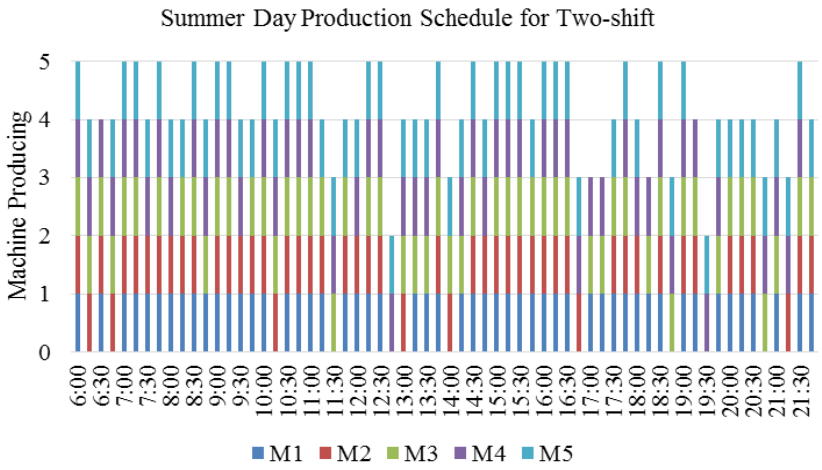

(a) The Optimal Production Schedule for Manufacturing System.

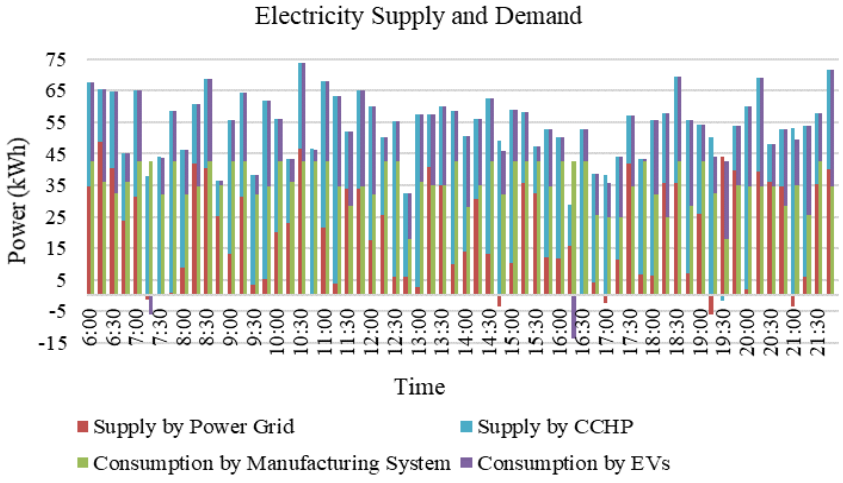

(b) The Electricity Supply and Demand Curve.

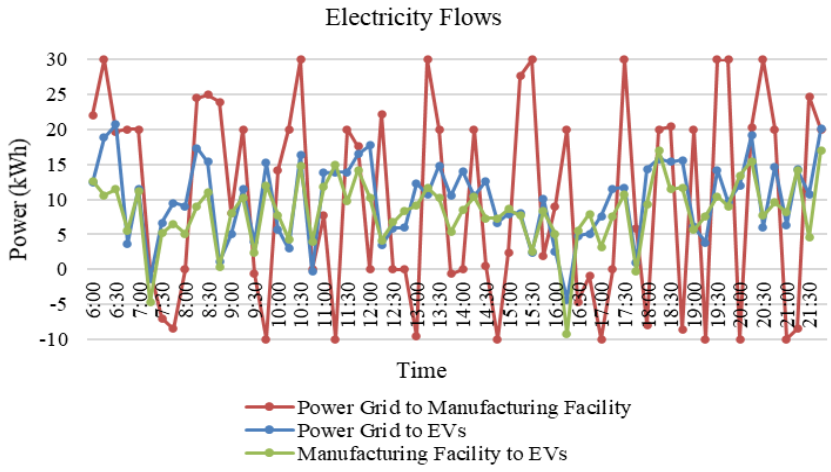

(c) the Electricity Flows.

Figure 12. The Optimized Solution of EPM System on the Summer Day for Two-Shift Production.

The cost components of the proposed EPM energy sharing system and baseline case results under the TOU tariff in the summer day for two-shift are reported in Table 15. The results in Table 15 indicate that the overall cost saving obtained from the optimal schedule is about 29.96% compared to the

baseline case. As shown in Tables 12 and 15, the proposed EPM energy sharing system can achieve more cost reduction than the baseline case for two-shift production in both the winter and summer days. Moreover, the summer day optimal solution cost saving is larger than the winter day optimal strategy cost reduction for two-shift production. The reason for this is that the cost for cooling energy demand can also be saved when production is adjusted to off-peak hours during summer days for two-shift production.

Table 15. The Cost (USD) Components between the Optimized Case and Baseline Case on the Summer Day for Two-Shift Production.

	Total Cost	Electricity		Fuel	Equipment		EVs Battery	Demand Charge
		Facility	EVs		CCHP	Boiler		
Optimized case	5185.95	111.24	113.83	481.60	205.62	-	410.85	3862.80
Baseline case	7404.47	317.25	130.92	479.25	-	39.04	177.50	6438.00
Cost saving	29.96%							

The CDE and PEC of the proposed overall system and baseline case are shown in Table 16 when the optimal strategy is adopted. As shown in Table 16, it is demonstrated that the proposed overall system in the winter day for two-shift is about 18.59% CDE reduction and 19.25% PEC saving than the baseline case, respectively. The CDE and PEC of the CCHP system in the EPM system are slightly larger than that of the boiler in the baseline case; while the power grid CDE and PEC are 47.87% and 48.06% lower than the baseline case.

Table 16. The *CDE* and *PEC* Comparison on the Summer Day for Two-Shift Production.

	CDE (tons)			*PEC* (kWh)		
	Total	Equipment	Power Grid	Total	Equipment	Power Grid
Optimized case	4.38	3.28	1.10	25,288.69	18,675.57	6613.12
Baseline case	5.38	3.27	2.11	31,316.77	18,584.40	12,732.37
Reduction	18.59%	−0.31%	47.87%	19.25%	−0.49%	48.06%

6. Conclusions and Future Work

In this paper, a cost-effective systematic framework under V2M operation is proposed. A collaborative model is presented to study energy sharing among the manufacturing facility, the EVs and the power grid under the TOU electricity tariff. The model is formulated in the format of a MINLP, aiming to minimize the total cost while maintaining the desired production target, and solved using PSO to obtain the optimal schedule of the CCHP system, manufacturing system, and EVs. The case study results show that the presented system can achieve 22.84% cost saving in the winter day for one-shift production, 34.81% in the summer day for one-shift production, 16.73% in the winter day for two-shift production, and 29.96% in the summer day for two-shift production compared with baseline cases. By adopting the optimal strategy, the CDE and PEC of the proposed collaborative system can be reduced by 22% and 23% in average, respectively. Therefore, the optimal solution for the proposed system has better economic, environmental, and energy performance compared with the ones obtained by the baseline cases.

This research is one of the first studies to explore the potential benefits of integrating EVs as energy storage units into manufacturing facilities. The synergies among the EVs, the manufacturing facilities and the electricity grid are proved to be viable and beneficial to enhance economic viability, energy efficiency, and environmental sustainability. Given the systematic modeling methodology adopted in this study, the proposed model can be further developed to a cost-effective decision-making tool to promote sustainable manufacturing.

In this study, although the most vital assumptions are all adopted, the presented model can be improved by considering more realistic and complex situations to further enhance the accuracy.

For future work, this research can be extended to consider uncertainties from the electricity price and EV driving schedules. In addition, the cost saving potentials can be investigated when other renewable energy sources are adopted to generate electricity in the manufacturing facilities.

Author Contributions: X.C. Conceptualization, Investigation, Validation, Writing—Original Draft. Y.G.: Conceptualization, Methodology, Writing—Review & Editing. X.Z. Visualization, Software. L.L. Conceptualization, Supervision, Writing—Review & Editing. D.Y. Formal analysis, Supervision. All authors have read and agreed to the published version of the manuscript.

Funding: This research received no external funding.

Conflicts of Interest: The authors declare that they have no known competing financial interests or personal relationships that could have appeared to influence the work reported in this paper.

Appendix A

Nomenclature

Indices			
t	index of the slotted interval, $t = 1, 2, \ldots, T$	i	index for the EVs, $i = 1, 2, \ldots, I$
n	index of the machines and buffers in the serial manufacturing production line, $n = 1, 2, \ldots, N$	q	set for equipment, $q = \{pgu, boiler, hc,\ cc\}$
Parameters			
P_t^{pur}	electricity price from power grid at time t (USD/kWh)	c	the air specific heat capacity (kWh/kg·°C)
P_t^{sell}	the selling price of electricity to power grid at time t (USD/kWh)	p	the density of air (kg/m^3)
P_t^f	the fuel price at time t (USD/kWh)	V	the volume of the manufacturing facility (m^3)
P_t^{trans}	electricity price between EVs and manufacturing facility at time t (USD/kWh)	a	PGU electric efficiency coefficient
A	capital recovery factor	b	PGU electric efficiency parameter
C_q^{cc}	unit investment cost of CCHP system equipment (USD/kWh)	η^{rec}	PGU heating efficiency
Cap	the capacity	η^{bo}	boiler heating efficiency
R^D	the demand charge ratio (USD/kW)	η^{hc}	heating component heating efficiency
r	the interest rate	η^{cc}	cooling component heating efficiency
y	number of years of operation of the system	Qh_t^{hw}	the manufacturing facility hot water demand at time t (kWh)
ONP	peak electricity time horizon	P^{ev}	each cycle cost price for every EV (USD)
Δt	15 min time interval (h)	$\eta^{ev,ch}$	EVs charging efficiency
CA_n	the capacity of the buffer n	$\eta^{ev,disch}$	EVs discharging efficiency
PR_n	the machine n production rate (units/h)	S_i	battery capacity of EV i
EFF_n	The machine n efficiency (%)	α_i^{cmin}	minimal charging limit of EV i
PT	the target of the producing period (units)	α_i^{cmax}	maximal charging limit of EV i
D_n	electricity demand of machine n (kWh)	α_i^{dmin}	minimal discharging limit of EV i
$\eta_n^{station}$	the efficiency of machine n	α_i^{dmax}	maximal discharging limit of EV i
cs	the convective of each machine	SOC_i^{arv}	battery electricity at arrive time of EV i
s_t	the radiant time series	SOC_i^{min}	minimal electricity store rate of EV i
Tem_t^{in}	expected indoor temperature (°C)	SOC_i^{max}	maximal electricity store rate of EV i
Tem_t^{out}	outdoor temperature (°C)	SOC_i^{dep}	The demand electricity at departure time of EV i
Decision variables (in time period t)			
$ef_t^{grid,mf}$	electricity flow from power grid to manufacturing facility (kWh)	CQ_t	the heat transferred from the manufacturing operation
$ef_t^{mf,grid}$	electricity flow from manufacturing facility to power grid (kWh)	Q_t^{sh}	the heating demand to be added except for the manufacturing operation
f_t^{pgu}	the fuel consumption by PGU (kWh)	Q_t^{sc}	the cooling demand to be added except for the manufacturing operation
f_t^{boiler}	the boiler fuel consumption (kWh)	q_t^{hc}	heat consumption of heat exchanger
$ef_{i,t}^{ev,mf}$	electricity from EV i to manufacturing facility (kWh)	q_t^{cc}	heat consumption of absorption chiller

$ef_{i,t}^{mf,ev}$	electricity from manufacturing facility to EV i (kWh)	$ef_{i,t}^{grid,ev}$	electricity from power grid to EV i
$B_{n,t}$	the buffer n contents at the beginning of time t	$ef_{i,t}^{ev,grid}$	electricity from EV i to power grid
ef_t^{pgu}	the PGU generate electricity (kWh)	$ef_{i,t}^{ev,ch}$	electricity charged in the EV i
GQ_t	the heat generated due to the manufacturing operation	$ef_{i,t}^{ev,disch}$	electricity discharged in the EV i
CQ_t^c	the heat transferred by instantaneous convection from the manufacturing operation	$es_{i,t}$	stored electricity of the EV i
CQ_t^r	the radiant heat transferred from the manufacturing operation		
	Binary decision variables (in time period t)		
$x_{n,t}$	1 if machine n is producing; 0 otherwise	Z_t^{cool}	1 if the manufacturing facility need cooling; 0 otherwise
Z_t^{sh}	1 if indoor temperature no less than outdoor temperature except for manufacturing system; 0 otherwise	$xc_{i,t}$	charging stage of EV i
Z_t^{sc}	1 if indoor temperature small than outdoor temperature except for manufacturing system; 0 otherwise	$xd_{i,t}$	discharging state of EV i
Z_t^{heat}	1 if the manufacturing facility need heating; 0 otherwise		

References

1. International Energy Agency. *Global Energy and CO2 Status Report*; International Energy Agency: Paris, France, 2018.
2. United States Environmental Protection Agency. *Global Greenhouse Gas Emissions Data, Greenhouse Gas (GHG) Emissions*; United States Environ. Prot. Agency: Washington, DC, USA, 2019.
3. Revesz, R.L.; Howard, P.H.; Arrow, K.; Goulder, L.H.; Kopp, R.E.; Livermore, M.A.; Oppenheimer, M.; Sterner, T. Global warming: Improve economic models of climate change. *Nature* **2014**, *508*, 173–175. [CrossRef] [PubMed]
4. Gaussin, M.; Hu, G.; Abolghasem, S.; Basu, S.; Shankar, M.R.; Bidanda, B. Assessing the environmental footprint of manufactured products: A survey of current literature. *Int. J. Prod. Econ.* **2013**, *146*, 515–523. [CrossRef]
5. Guan, X.; Zhang, H.; Xue, C. A method of selecting cold and heat sources for enterprises in an industrial park with combined cooling, heating, and power. *J. Clean. Prod.* **2018**, *190*, 608–617. [CrossRef]
6. Ge, Y.; Li, L. System-level energy consumption modeling and optimization for cellulosic biofuel production. *Appl. Energy* **2018**, *226*, 935–946. [CrossRef]
7. Zhang, S.; Gajpal, Y.; Appadoo, S.S.; Abdulkader, M.M.S. Electric vehicle routing problem with recharging stations for minimizing energy consumption. *Int. J. Prod. Econ.* **2018**, *203*, 404–413. [CrossRef]
8. Zhao, X.; Doering, O.C.; Tyner, W.E. The economic competitiveness and emissions of battery electric vehicles in China. *Appl. Energy* **2015**, *156*, 666–675. [CrossRef]
9. Ren, S.; Luo, F.; Lin, L.; Hsu, S.C.; LI, X.I. A novel dynamic pricing scheme for a large-scale electric vehicle sharing network considering vehicle relocation and vehicle-grid-integration. *Int. J. Prod. Econ.* **2019**, *218*, 339–351. [CrossRef]
10. International Energy Agency; Global, E.V. *Outlook 2017*; International Energy Agency: Paris, France, 2017.
11. Becker, T.T.A.T.; Sidhu, I.; Tenderich, B. *Electric Vehicles in the United States: A New Model with Forecasts to 2030*; Center for Entrepreneurship & Technology: University of California, Berkeley, Berkeley, CA, USA, 2009.
12. Fairley, P. Speed bumps ahead for electric-vehicle charging. *IEEE Spectr.* **2010**, *47*, 13–14. [CrossRef]
13. Nejad, M.M.; Mashayekhy, L.; Chinnam, R.B.; Grosu, D. Online scheduling and pricing for electric vehicle charging. *IISE Trans.* **2017**, *49*, 178–193. [CrossRef]
14. Wang, S.; Tang, R. Supply-based feedback control strategy of air-conditioning systems for direct load control of buildings responding to urgent requests of smart grids. *Appl. Energy* **2017**, *201*, 419–432. [CrossRef]

15. Sedighizadeh, M.; Esmaili, M.; Mohammadkhani, N. Stochastic multi-objective energy management in residential microgrids with combined cooling, heating, and power units considering battery energy storage systems and plug-in hybrid electric vehicles. *J. Clean. Prod.* **2018**, *195*, 301–317. [CrossRef]
16. Heymans, C.; Walker, S.B.; Young, S.B.; Fowler, M. Economic analysis of second use electric vehicle batteries for residential energy storage and load-levelling. *Energy Policy* **2014**, *71*, 22–30. [CrossRef]
17. Sortomme, E.; El-Sharkawi, M.A. Optimal charging strategies for unidirectional vehicle-to-grid. *IEEE Trans. Smart Grid* **2011**, *2*, 131–138. [CrossRef]
18. Sassi, O.; Oulamara, A. Electric vehicle scheduling and optimal charging problem: Complexity, exact and heuristic approaches. *Int. J. Prod. Res.* **2017**, *55*, 519–535. [CrossRef]
19. Wang, R.; Li, Y.; Wang, P.; Niyato, D. Design of a V2G aggregator to optimize PHEV charging and frequency regulation control. In Proceedings of the 2013 IEEE International Conference on Smart Grid Communications, SmartGridComm 2013, Vancouver, BC, Canada, 21–24 October 2013.
20. Hegazy, O.; Van Mierlo, J.; Lataire, P. Design and control of bidirectional DC/AC and DC/DC converters for plug-in hybrid electric vehicles. In Proceedings of the International Conference on Power Engineering, Energy and Electrical Drives, Malaga, Spain, 10–12 May 2011.
21. El, R.A.; Selim, F.; Bentouati, B.; Abido, M.A. A novel multi-objective hybrid particle swarm and salp optimization algorithm for technical-economical-environmental operation in power systems. *Energy* **2020**, *193*, 116817. [CrossRef]
22. Moradijoz, M.; Parsa Moghaddam, M.; Haghifam, M.R.; Alishahi, E. A multi-objective optimization problem for allocating parking lots in a distribution network. *Int. J. Electr. Power Energy Syst.* **2013**, *46*, 115–122. [CrossRef]
23. Lin, X.; Sun, J.; Ai, S.; Xiong, X.; Wan, Y.; Yang, D. Distribution network planning integrating charging stations of electric vehicle with V2G. *Int. J. Electr. Power Energy Syst.* **2014**, *63*, 507–512. [CrossRef]
24. Liang, H.; Liu, Y.; Li, F.; Shen, Y. Dynamic Economic/Emission Dispatch Including PEVs for Peak Shaving and Valley Filling. *IEEE Trans. Ind. Electron.* **2019**, *66*, 2880–2890. [CrossRef]
25. Saber, A.Y.; Venayagamoorthy, G.K. Intelligent unit commitment with vehicle-to-grid—A cost-emission optimization. *J. Power Sources* **2010**, *195*, 898–911. [CrossRef]
26. Islam, F.R.; Pota, H.R.; Anwar, A.; Nasiruzzaman, A.B.M. Design a unified power quality conditioner using V2G technology. In Proceedings of the 2012 IEEE International Power Engineering and Optimization Conference, PEOCO 2012—Conference Proceedings, Melaka, Malaysia, 6–7 June 2012.
27. Iacobucci, R.; McLellan, B.; Tezuka, T. Modeling shared autonomous electric vehicles: Potential for transport and power grid integration. *Energy* **2018**, *158*, 148–163. [CrossRef]
28. Bashash, S.; Fathy, H.K. Cost-optimal charging of plug-in hybrid electric vehicles under time-varying electricity price signals. *IEEE Trans. Intell. Transp. Syst.* **2014**, *15*, 1958–1968. [CrossRef]
29. Ghofrani, M.; Arabali, A.; Etezadi-Amoli, M.; Fadali, M.S. Smart scheduling and cost-benefit analysis of grid-enabled electric vehicles for wind power integration. *IEEE Trans. Smart Grid* **2014**, *5*, 2306–2313. [CrossRef]
30. Tan, K.M.; Ramachandaramurthy, V.K.; Yong, J.Y. Integration of electric vehicles in smart grid: A review on vehicle to grid technologies and optimization techniques. *Renew. Sustain. Energy Rev.* **2016**, *53*, 720–732. [CrossRef]
31. Pang, C.; Dutta, P.; Kezunovic, M. BEVs/PHEVs as dispersed energy storage for V2B uses in the smart grid. *IEEE Trans. Smart Grid* **2012**, *3*, 473–482. [CrossRef]
32. Karan, E.; Mohammadpour, A.; Asadi, S. Integrating building and transportation energy use to design a comprehensive greenhouse gas mitigation strategy. *Appl. Energy* **2016**, *165*, 234–243. [CrossRef]
33. Stadler, M.; Kloess, M.; Groissböck, M.; Cardoso, G.; Sharma, R.; Bozchalui, M.C.; Marnay, C. Electric storage in California's commercial buildings. *Appl. Energy* **2013**, *104*, 711–722. [CrossRef]
34. Sharafi, M.; ElMekkawy, T.Y.; Bibeau, E.L. Optimal design of hybrid renewable energy systems in buildings with low to high renewable energy ratio. *Renew. Energy* **2015**, *83*, 1026–1042. [CrossRef]
35. Ioakimidis, C.S.; Thomas, D.; Rycerski, P.; Genikomsakis, K.N. Peak shaving and valley filling of power consumption profile in non-residential buildings using an electric vehicle parking lot. *Energy* **2018**, *148*, 148–158. [CrossRef]

36. Van Roy, J.; Leemput, N.; Geth, F.; Buscher, J.; Salenbien, R.; Driesen, J. Electric vehicle charging in an office building microgrid with distributed energy resources. *IEEE Trans. Sustain. Energy* **2014**, *5*, 1389–1396. [CrossRef]
37. Davidov, S.; Pantoš, M. Planning of electric vehicle infrastructure based on charging reliability and quality of service. *Energy* **2017**, *118*, 1156–1167. [CrossRef]
38. Un-Noor, F.; Padmanaban, S.; Mihet-Popa, L.; Mollah, M.N.; Hossain, E. A comprehensive study of key electric vehicle (EV) components, technologies, challenges, impacts, and future direction of development. *Energies* **2017**, *10*, 1217. [CrossRef]
39. Wu, X.; Hu, X.; Teng, Y.; Qian, S.; Cheng, R. Optimal integration of a hybrid solar-battery power source into smart home nanogrid with plug-in electric vehicle. *J. Power Sources* **2017**, *363*, 277–283. [CrossRef]
40. Quddus, M.A.; Shahvari, O.; Marufuzzaman, M.; Usher, J.M.; Jaradat, R. A collaborative energy sharing optimization model among electric vehicle charging stations, commercial buildings, and power grid. *Appl. Energy* **2018**, *229*, 841–857. [CrossRef]
41. Wang, Z.; Wang, L.; Dounis, A.I.; Yang, R. Integration of plug-in hybrid electric vehicles into energy and comfort management for smart building. *Energy Build.* **2012**, *47*, 260–266. [CrossRef]
42. U.S. Energy Information Administration. *U.S. Energy-Related Carbon Dioxide Emissions in U.S. Manufacturing*; U.S. Energy Information Administration: Washington, DC, USA, 2018.
43. Dababneh, F.; Li, L.; Sun, Z. Peak power demand reduction for combined manufacturing and HVAC system considering heat transfer characteristics. *Int. J. Prod. Econ.* **2016**, *177*, 44–52. [CrossRef]
44. Ge, Y.; Li, L.; Wang, Y. Modeling of Bernoulli production line with the rework loop for transient and steady-state analysis. *J. Manuf. Syst.* **2017**, *44*, 22–41. [CrossRef]
45. Yang, J.; He, L.; Fu, S. An improved PSO-based charging strategy of electric vehicles in electrical distribution grid. *Appl. Energy* **2014**, *128*, 82–92. [CrossRef]
46. Kennedy, J.; Eberhart, R. Particle swarm optimization. In Proceedings of the ICNN'95-International Conference on Neural Networks, Perth, WA, Australia, 27 November–1 December 1995. [CrossRef]
47. Al-Bahrani, L.T.; Patra, J.C. Multi-gradient PSO algorithm for optimization of multimodal, discontinuous and non-convex fuel cost function of thermal generating units under various power constraints in smart power grid. *Energy* **2018**, *147*, 1070–1091. [CrossRef]
48. Maiyar, L.M.; Thakkar, J.J. Modelling and analysis of intermodal food grain transportation under hub disruption towards sustainability. *Intern. J. Prod. Econ.* **2019**, *217*, 281–297. [CrossRef]
49. Eberhart, R.C.; Shi, Y. Particle swarm optimization: Developments, applications and resources. In Proceedings of the IEEE Conference on Evolutionary Computation, ICEC, Seoul, Korea, 27–30 May 2001.
50. Shi, Y.; Eberhart, R.C. Empirical study of particle swarm optimization. In Proceedings of the 1999 Congress on Evolutionary Computation, CEC 1999, Washington, DC, USA, 6–9 July 1999.
51. Shi, Y.; Eberhart, R. A modified particle swarm optimizer. In Proceedings of the 1998 IEEE International Conference on Evolutionary Computation Proceedings. IEEE World Congress on Computational Intelligence (Cat. No. 98TH8360), Anchorage, AK, USA, 4–9 May 1998.
52. Chen, G. Study on the Strategy of Decreasing Inertia Weight in Particle Swarm Optimization Algorithm. *J. Xi'Jiaotong Univ.* **2006**, *40*, 53.
53. Huang, B.; Bai, L.; Roy, A.; Ma, N. A multi-criterion partner selection problem for virtual manufacturing enterprises under uncertainty. *Int. J. Prod. Econ.* **2018**, *196*, 68–81. [CrossRef]
54. Wang, L.; Wang, Z.; Yang, R. Intelligent multiagent control system for energy and comfort management in smart and sustainable buildings. *IEEE Trans. Smart Grid* **2012**, *3*, 605–617. [CrossRef]
55. Brundage, M.P.; Chang, Q.; Chen, D.; Yu, V. Energy savings opportunities of an integrated facility and production line. In Proceedings of the ASME 2013 International Manufacturing Science and Engineering Conference Collocated with the 41st North American Manufacturing Research Conference, MSEC 2013, Madison, WI, USA, 10–14 June 2013.
56. Bruning, S.F. A New Way to Calculate Cooling Loads. *ASHRAE J.* **2004**, *46*, 20.
57. Liu, M.; Shi, Y.; Fang, F. Optimal power flow and PGU capacity of CCHP systems using a matrix modeling approach. *Appl. Energy* **2013**, *102*, 794–802. [CrossRef]
58. Dai, R.; Hu, M.; Yang, D.; Chen, Y. A collaborative operation decision model for distributed building clusters. *Energy* **2015**, *84*, 759–773. [CrossRef]

59. Kuang, Y.; Chen, Y.; Hu, M.; Yang, D. Influence analysis of driver behavior and building category on economic performance of electric vehicle to grid and building integration. *Appl. Energy* **2017**, *207*, 427–437. [CrossRef]
60. Pacific Gas and Electric Tariff-Regulatory Documents | PGE. Available online: https://www.portlandgeneral.com/our-company/regulatory-documents/tariff (accessed on 13 June 2020).
61. Weather Underground. San Francisco, CA Weather History | Weather Underground. Available online: https://www.wunderground.com/history/monthly/us/ca/san-francisco/KSFO (accessed on 13 June 2020).
62. Hang, Y.; Qu, M.; Zhao, F. Economic and environmental life cycle analysis of solar hot water systems in the United States. *Energy Build.* **2012**, *45*, 181–188. [CrossRef]